J. Fluid Mech. (1994), *vol.* 277, *pp.* 135–162

The generation and regeneration of single hairpin vortices

By A. H. HAIDARI† AND C. R. SMITH
Department of Mechanical Engineering and Mechanics, Lehigh University, Bethlehem, PA 18015, USA

(Received 10 August 1993 and in revised form 10 May 1994)

The generation and growth of single hairpin vortices created by controlled surface fluid injection were examined experimentally within a laminar boundary layer over a range of Reynolds numbers. Flow visualization, using both dye and hydrogen bubbles, was employed in conjunction with hot-film anemometry to investigate the growth characteristics and evolution of these single hairpin vortices. Hydrogen-bubble visualization results reveal that the passage of a hairpin vortex can give rise to a low-speed streak pattern adjacent to the surface, and a turbulent pocket-like pattern farther removed from the surface. When the displacement and injection Reynolds numbers exceed critical levels, regeneration processes occur, which result in the development of new hairpin-like vortices by both (i) lateral deformation of the vortex lines comprising the initial hairpin vortex and (ii) a process of vortex–surface interaction, which causes the ejection of surface fluid and subsequent hairpin formation by viscous–inviscid interactions. The combination of these processes results in both lateral and streamwise growth of the initial hairpin-vortex structure, yielding a symmetric turbulent-spot type of behaviour.

1. Introduction

1.1. *General*

As the result of extensive research on turbulent flows, particularly flat-plate flows, it has become evident that turbulence is composed of numerous scales and flow structures that are generated and interact by means of complex three-dimensional vortex dynamics. Detailed studies over the past two decades suggest that turbulent boundary layers are sustained by an ordered (but complex) cyclic sequence of events which takes place in the flow near the wall. This apparently deterministic sequence of events is usually referred to as the coherent structure or the coherent behaviour of the flow.

In the region close to the wall, two universally accepted features which appear to dominate the dynamics of the wall-layer flow are (i) the ubiquitous low-speed streaks, characteristic of turbulent boundary-layer flows (Kline *et al.* 1967; Smith & Metzler 1983; Robinson 1991), and the bursting event, wherein wall-layer fluid is observed to erupt into the outer region of the flow at isolated spanwise and streamwise locations (Kim, Kline & Reynolds 1971; Robinson 1991). It is widely believed (e.g. Kim *et al.* 1971; Robinson 1991) that the oscillation and lift-up of the low-speed streaks precedes an eruption of the wall-layer fluid in a bursting event. This relationship between the low-speed streaks and the burst events has motivated a number of studies attempting to establish a characteristic flow structure(s) which can explain the events observed in

† Presently employed at Fluent Inc., Lebanon, N.H. 03766.

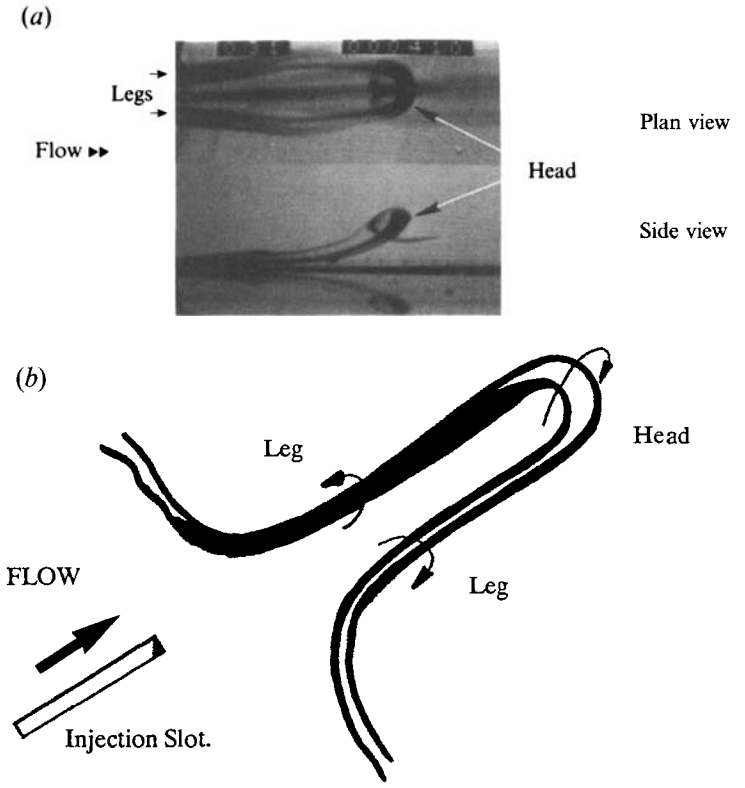

FIGURE 1. (*a*) Dual view of a dye-marked single hairpin vortex. (*b*) Isometric schematic of a single hairpin vortex following generation.

a turbulent boundary layer. Among the various proposed flow structures, hairpin-like vortices are one of the most promising models of a typical flow structure in a turbulent boundary layer (Smith *et al.* 1991).

From a growing list of researchers who have suggested hairpin-type vortices as a basic flow structure of turbulent boundary layers, the following are believed to have uniquely contributed: Theodorsen (1952), Willmarth & Tu (1967), Offen & Kline (1975), Head & Bandyopadhyay (1981), Perry & Chong (1982), Smith (1984), Kim (1987), Acarlar & Smith (1987*a*, *b*), Smith *et al.* (1991), and Robinson (1991). A variety of terms have been used to describe hairpin vortices (e.g. horseshoe and loop vortices); here the term 'hairpin' will be used to denote any vortex having the characteristic shape indicated in figure 1. The tip of a hairpin vortex is referred to as the vortex head, while the portions of the vortex that are mainly aligned in the streamwise direction and close to the wall are termed the vortex legs. Note that figure 1(*b*) is for illustration purposes only and that the vortex legs may not terminate as shown. In fact, in a turbulent boundary layer the symmetry of the vortex will be predominantly distorted, yielding what Robinson (1991) has termed 'one-legged hairpins'.

In a study of the effects of three-dimensional flows, Theodorsen (1952) used the vorticity transport equation combined with a physical understanding of vortex dynamics to hypothesize that a horseshoe-shaped vortex is a key structure in the energy transport within a turbulent boundary layer. He inferred that a turbulent flow structure must be three-dimensional and inclined near 45° to the surface in order to maximize turbulence production relative to dissipation. He conjectured that any new turbulent

structure should be similar in pattern to the primary turbulence structure, but of smaller scale; this latter point has been crystallized in a unique modelling of turbulent boundary layers by Perry & Chong (1982) and Perry, Henbest & Chong (1986).

Following Theodorsen, a number of other researchers have proposed hairpin-like structures in turbulent boundary layers (Willmarth & Tu 1967; Offen & Kline 1975; Head & Bandyopadhyay 1981; Perry & Chong 1982; Wallace 1983; Smith 1984). Head & Bandyopadhyay (1981) were the first researchers to actually detect what appeared to be hairpin-like vortices in a fully developed turbulent boundary layer using smoke visualization and hot-film measurements.

The origin of hairpin vortices and the physical description of the cause-and-effect of bursting in a turbulent boundary layer were the motivation for a flow model suggested by Smith (1984). The model was based on extensive visualization experiments, as well as previous models due to Offen & Kline (1975), Willmarth & Tu (1967), and Wallace (1983). Smith suggested that imposition of a local adverse pressure gradient caused by passage of a disturbance causes a local deceleration of a low-speed streak, which generates an inflection in the streamwise velocity profile near the interface between the streak and the high-speed outer-region fluid. The breakdown of this inflectional region was suggested to cause a three-dimensional vortex roll-up leading to the formation of one or more hairpin vortices. The bursting process was suggested to be due to the breakup of low-speed streaks, which in turn are believed to be generated by the viscous interaction of the counter-rotating legs of a hairpin vortex with the wall. This process of vortex–surface interaction has been documented in a series of studies by Walker and his students (e.g. Walker 1978; Peridier, Smith & Walker 1991), and forms the basis for a comprehensive model of turbulence proposed by Smith *et al.* (1991).

From the intuitive suggestion made by Theodorsen (1952) to the development of a more complete picture of flow activity by Smith *et al.* (1991), there have been many contributions to the current understanding of the origin of turbulence and its dominant flow structures. One useful approach which facilitates our understanding of turbulence structure has been the examination of the vortex dynamics of isolated vortex flow structures using 'kernel' studies (see Smith 1993), which are employed to infer the structure of turbulence by cross-comparison of the measured/observed behaviour of isolated flow structures with a fully turbulent flow.

One key kernel study was carried out by Acarlar & Smith (1987*a*, *b*), who performed a series of experiments in which hairpin vortices were artificially generated in a subcritical laminar flat-plate boundary layer. Using flow visualization and probe measurements, Acarlar & Smith illustrate that many of the flow patterns generated by advecting hairpin vortices appear markedly similar to fully developed turbulent-boundary-layer flow patterns. The similarities between the results for the train of hairpin vortices studied by Acarlar & Smith and a bounded turbulent flow provide strong support for the hypothesis that hairpin or hairpin-like vortices are integral flow structures within the wall region of a turbulent boundary layer.

In complementary studies, Hon & Walker (1987) and Sobrun (1994) consider hairpin vortex behaviour analytically/computationally, concentrating on understanding the dynamics of an advected hairpin vortex in a shear flow. They evaluate the development, growth, and interaction of hairpin vortices using a Lagrangian approach based on the numerical evaluation of the discretized Biot–Savart integral. They hypothesize that hairpin vortices are streak creators, and that an advecting hairpin vortex induces the concentration and eruption of the viscous flow near the wall in a manner similar to that observed with a turbulent-boundary-layer streak. This vortex-induced eruption process has been clearly demonstrated by Peridier *et al.* (1991), where

it is suggested that the generation of an eruptive response near the wall leads to the generation of new vortices through a strong viscous–inviscid interaction with the outer flow. Smith *et al.* (1991), through a synthesis of manifold experimental and computational studies of hairpin vortices, suggest that the creation of new hairpin vortices is a regenerative process, providing an explanation for how hairpin-type vortices continuously form within a turbulent boundary layer.

1.2. *Present study*

The complexities associated with the study of vortex flow structures in a turbulent-boundary-layer environment remain an obstacle to developing a universally accepted turbulent flow model. Thus, one rational approach is the further use of kernel-type experiments, as discussed above. The present experiments extend the continuous hairpin-vortex generation studies of Acarlar & Smith (1987) to the detailed study of single individually generated hairpin vortices. While Acarlar & Smith were able to show that a continuously generated train of hairpin vortices will give rise to many of the basic visualization and velocity patterns characteristically observed in a turbulent boundary layer, their study could not show how hairpin vortices behave individually nor the process of interaction which leads to the generation of subsequent flow structures, and thus sustaining wall turbulence.

Thus, the objectives of the present study were to experimentally create single hairpin vortices in a controlled laminar environment, and to establish the detailed processes of their subsequent evolution, including:

(i) the physical process involved in the formation of single hairpin vortices;
(ii) the kinematic characteristics of a single hairpin vortex following formation; and
(iii) the processes of hairpin vortex development, interaction, and regeneration.

2. Experimental arrangement

Experiments were conducted in a free-surface Plexiglas water channel at Lehigh University. The working section of the channel is 5 m long, 0.9 m wide and 0.4 m deep. The stable flow range of the channel is 0.03 to 0.4 m s^{-1}, with a spanwise flow uniformity of $\pm 2\%$. The present experiments were conducted over a velocity range of 0.05–0.21 m s^{-1}. A detailed description of the flow channel is provided by Acarlar & Smith (1987*a*).

The experiments were conducted using a 180 cm × 85 cm, 1.9 cm thick Plexiglas false-bottom test plate with a 5:1 elliptical leading edge; a side-view schematic of the test-plate is shown in figure 2 (see Haidari 1990 for further details). A streamwise fluid injection slot was located 45 cm from the leading edge; a series of injection plugs were constructed and examined to determine the effect of different injection slot geometry on effective hairpin generation. A series of dye visualization studies established that slot geometry strongly affects the generation of single hairpin vortices (see Haidari 1990), with injection from a diffuser-type injection slot providing the most consistent and symmetric generation of hairpin vortices. The majority of the results presented in this study are obtained with a 2 mm wide slot; a 1 mm slot was also employed for a limited set of studies (see Haidari 1990). To generate a hairpin vortex, fluid was introduced at the bottom of a reservoir in the injection plug, where a miniature distribution manifold and a porous sponge distributed fluid uniformly across the injection slot, creating a uniform slot injection profile.

The creation of repeatable single hairpin vortices is directly related to the quality of the injection system. The present injection system, shown in figure 2 (see also Haidari

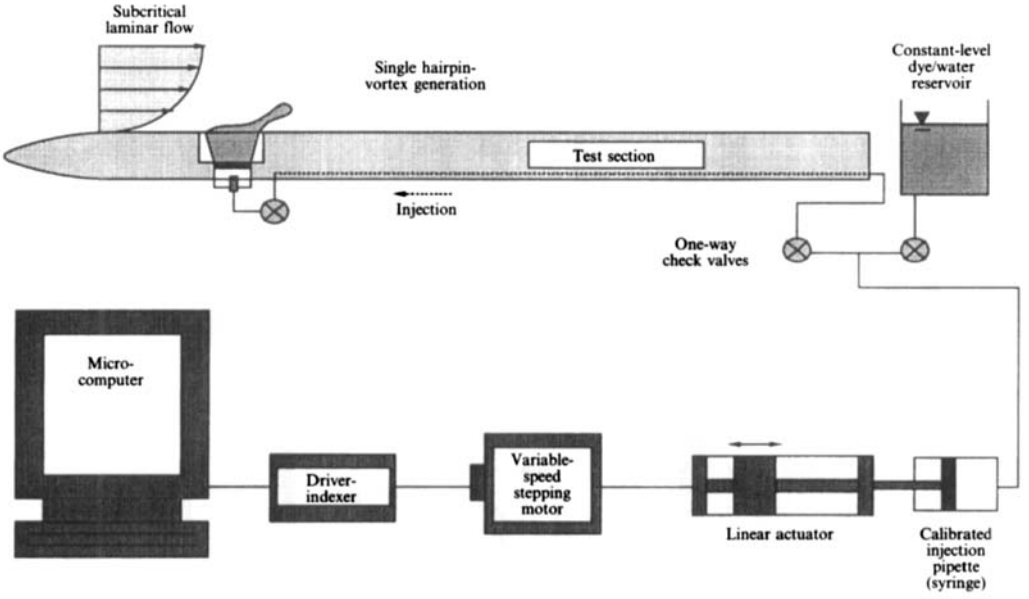

FIGURE 2. Schematic of the controlled injection system.

1990), employs a Compumotor drive of a linear actuator, which in turn controls the stroke of a calibrated syringe. The motor is controlled by an in-house computer program; phase referencing is accomplished using a specially designed optoelectronics circuit. This system provides a prescribed amount of injection fluid at a prescribed velocity on the forward stroke of the syringe; during the suction stroke, fluid from a constant-level reservoir fills the syringe for the next injection. As shown in figure 2, one-way check valves are used to prevent a reflux of fluid from the injection slot during the suction half of the syringe cycle.

Flow visualization and hot-film anemometry were used to provide both qualitative and quantitative analysis of hairpin-vortex flow characteristics. Visualization of the flow structures was done using both dye and hydrogen-bubble visualization techniques. The visualization data were recorded with an INSTAR high-speed video system (120 frames s^{-1}) described in previous publications (e.g. Acarlar & Smith 1987*a*).

Hairpin vortices and their development could be visualized in plan, side and end views; simultaneous two-camera viewing using split-screen effects allowed combined plan–side, or plan–end views to be obtained. A schematic diagram of the camera orientation employed for both plan- and end-view visualization is shown in figure 3. General lighting was provided by either a strobe light or a studio lamp located beneath the channel. A series of experiments was also conducted using a scanned, 1 mm laser light sheet, created using a 5 W Argon laser and a controlled frequency scanning mirror.

The velocity characteristics of a passing hairpin vortex and its associated flow structure were measured with Dantec type 55M10 anemometers, using both a single element R-11 and a x-film R-63 probe. Probe calibration was accomplished by towing the probe through a quiescent water channel using an overhead traversing instrumentation platform (see Smith & Metzler 1983; Haji-Haidari & Smith 1988).

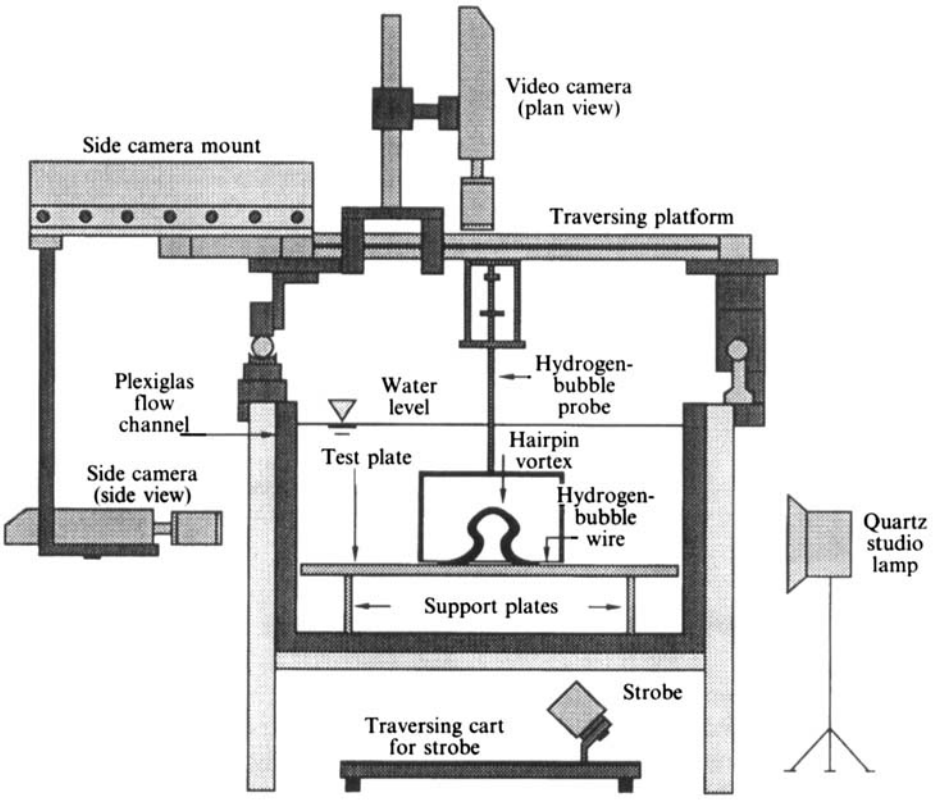

FIGURE 3. Schematic representation of the camera locations for side and plan views; looking upstream, with the test section and hydrogen-bubble probe in place.

3. The generation and characteristics of single hairpin vortices

3.1. *Introduction*

The results obtained address the behaviour of a single hairpin vortex at various levels of development over a wide range of flow conditions, and are divided into two categories. The present section describes the process of single hairpin-vortex generation and the initial characteristics of a single hairpin vortex. The results related to the growth and the development of single vortices are examined subsequently in §§4 and 5.

3.2. *Vortex generation*

The controlled injection process was examined over a wide range of both plate and injection Reynolds numbers to establish the regime within which stable single hairpin vortices can be generated. Figure 1 (*a*), photographed from a video sequence, is a dual-view picture of a stable single hairpin vortex structure. Visualized by dye in the injected fluid, the combined views of figure 1 (*a*) and the schematic of figure 1 (*b*) illustrate some of the features commonly associated with hairpin vortices.

The head of the vortex has a clockwise rotation about the cross-stream axis. From the hairpin head, the vortex tube bends around and connects to the upstream-trailing counter-rotating legs, which are elongated in the streamwise direction at a shallow angle to the surface, with their axes of rotation generally aligned with the flow direction. Note that figure 1 (*a*) is obtained immediately downstream of the injection slot; as will be shown in §3.4, the vortex structure undergoes continuous change as it advects downstream.

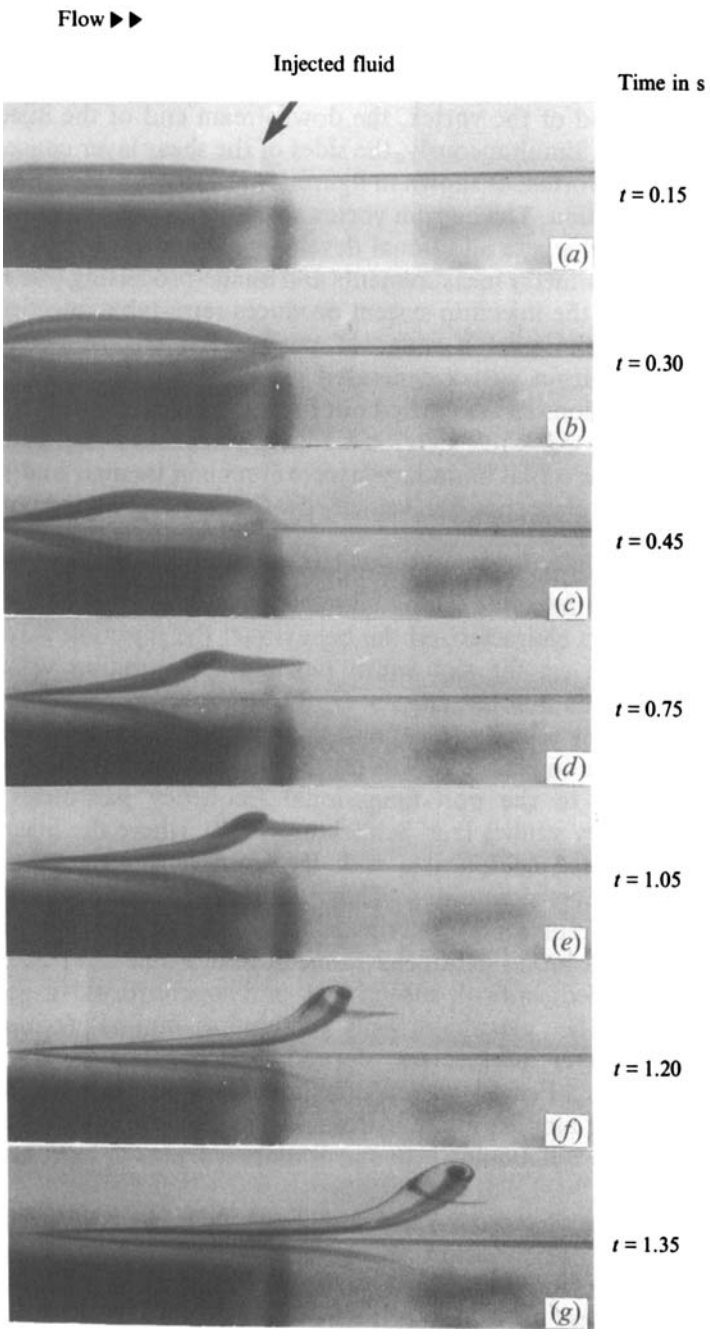

FIGURE 4. Dye visualization of a single hairpin-vortex generation, $Re_{\delta^*} = 354$.

Figure 4 is a sequence of side-view dye visualization photographs, illustrating the temporal formation of a typical single hairpin vortex by controlled fluid injection through a streamwise slot. Figure 4(*a*) shows the initiation of fluid injection from the slot. The fluid continues to penetrate outward from the surface (figure 4*b*) until cessation of the injection fluid (at $t = 0.30$ s). The shear layer which forms between the injected fluid and the displaced boundary-layer fluid interacts with the outer flow (a

more detailed discussion will follow) and a vortex begins to roll up from the upstream side of the injection (figures 4*c* and 4*d*). Note that during this timespan, downstream advection of the injected fluid (as visualized by the dye marker) is limited. As the shear layer rolls into the head of the vortex, the downstream end of the injected fluid lifts away from the surface. Simultaneously, the sides of the shear layer concentrate and tilt to form the legs of the vortex, as shown in figures 4(*d*) and 4(*e*), with the legs elongated in the streamwise direction. The hairpin vortex structure formed accelerates, advecting downstream (figure 4*g*) where additional development and growth take place.

Using hot-film anemometry measurements and image-processing (see Haidari 1990), it was established that the injection system produces repeatable injection and hairpin generation characteristics over a range of parameters, resulting in identical flow behaviour for each hairpin vortex generated under fixed conditions. In addition, a series of flow visualization studies carried out for the range of Reynolds number based on streamwise distance $2.3 \times 10^4 < Re_x < 8.8 \times 10^4$ established that in the absence of the injection process the initial boundary layer will remain laminar and stable over the entire length of the test plate; hot-film velocity profiles indicated good comparison with accepted Blasius behaviour.

The generation of hairpin vortices is strongly affected by the rate and the volume of the injection as well as the approaching boundary-layer characteristics. In the present study, three parameters characterized the behaviour: the injection Reynolds number ($Re_{Vw} = V_w w/\nu$) based on the slot width (w) and the injection velocity (V_w); the approach-flow Reynolds number ($Re_{\delta^*} = U_\infty \delta^*/\nu$) based on displacement thickness (δ^*) and the free-stream velocity (U_∞); and the non-dimensional injection parameter (δ^*/tU_∞) based on the injection period (t). Note that the injection parameter was chosen to be similar to the non-dimensional frequency parameter employed in boundary-layer stability studies (e.g. Schlichting 1978), where the injection period of this study (t) is assumed comparable with the inverse of the excitation frequency employed in stability considerations. Thus, Re_{δ^*} and δ^*/tU_∞ are consistent with stability studies; Re_{Vw} represents a parameter unique to the present injection study. A systematic study over a broad parameter range indicates that three hairpin formation regimes can be identified: critical, subscritical, and supercritical. In general, a single hairpin vortex will be generated only within a limited (critical) range of injection–boundary layer parameters, depending most heavily on the injection Reynolds number, Re_{Vw}. For a low Re_{Vw}, the interaction of the injected fluid with the boundary layer will not amplify into a hairpin-vortex structure (subcritical); for higher Re_{Vw}, the injected fluid will amplify into one or more hairpins or hairpin-like structures (supercritical).

To establish the range for critical regime behaviour, an extensive parametric study was done using flow visualization to characterize the regime. The criterion for accepting a vortex as a single hairpin vortex was that the generated structure must be similar in shape to that of figure 1, with no other flow structures preceding or succeeding the generated vortex. Figure 5 shows data obtained using a 2 mm wide slot which fall in the critical single-hairpin regime. The procedure for establishing the regime behaviour was as follows. With the plate Reynolds number fixed, either the volume of fluid injection was systematically increased, or the time of injection (t) was decreased, both of which vary the injection velocity, V_w. When a critical lower limit was reached for a particular Re_{δ^*}, single hairpin vortices would begin to form; this point corresponds to the lowest Re_{Vw} shown in figure 5. Similarly, the maximum Re_{Vw} shown is the upper limit of injection parameters where a single hairpin vortex could still be generated; beyond these characteristics, the injection process would form multiple

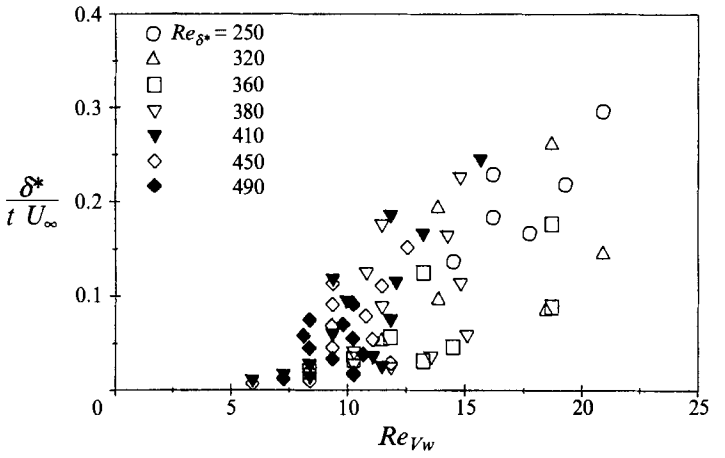

FIGURE 5. Parametric ranges over which single hairpin vortices could be generated for a 2 mm thick injection slot.

hairpin vortices. The reduction in the range of injection parameters with increasing Reynolds number, as illustrated in figure 5, implies that at higher Reynolds number only low volumetric injections of short duration will generate single hairpin vortices. This is clearly due to the reduced stability of the bound shear layer with increasing Reynolds number.

3.3. *Single hairpin-vortex formation*

The roll-up of single hairpin vortices was visualized using both dye and hydrogen bubbles. Vertical and horizontal hydrogen-bubble wires were systematically located at a series of strategic positions in the vicinity of the injection slot, and the resulting flow patterns were observed from plan, side, and end view, as well as in combined plan–end, and plan–side views.

Hairpin-vortex formation due to injection from a streamwise slot is a complicated process. The injected fluid alters the flow field in time and space as well as introducing new vorticity from the injection process itself. It is reasonable to think of the injection slot as a weak jet which forms an elongated concentrated sheet of vorticity with an aspect ratio of approximately 30:1 as it leaves the injection slot. This sheet of vorticity is introduced into the high-shear region of the boundary layer near the wall where the vorticity rapidly redistributes itself within the boundary layer.

As shown in the dye-visualized picture sequence of figure 4, the boundaries which encompass the injected fluid (dye marked) continuously change under the action of inertial as well as shear forces. At the completion of the injection (figure 4*b*), the fluid at the upstream end accelerates forward, initiating deformation of the interface as shown in figure 4(*b*–*g*). As the shear layer between the injected fluid and the free stream rolls up, the fluid on the symmetry plane continues to move away from the surface and experiences continued acceleration by the high-speed outer flow. The continued roll-up of the upper shear layer culminates in the formation of a transverse vortex (completed by approximately figure 4*f*), comprising the head of the hairpin vortex. This hairpin vortex head connects back upstream through the vertical shear layer formed to either side of the slot by the injection. Tilting, stretching, and roll-up of this vertical shear layer results in the formation of the legs of the hairpin vortex, which extend in the flow direction, describing a shallow angle to the surface.

Close to the surface, the low-speed injected fluid causes higher-speed fluid

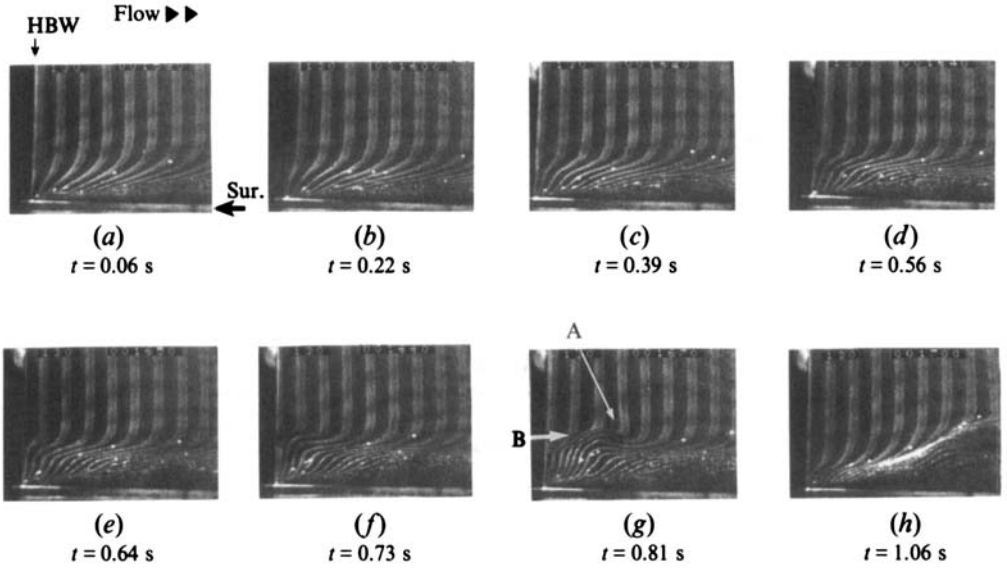

FIGURE 6. Side-view sequence of hydrogen-bubble-wire (HBW) visualization on the symmetry plane of the injection slot during the formation of a single hairpin vortex. $x_{wire} = 1.0$ cm. $U_0 = 8.8$ cm s^{-1}, $\delta^* = 0.4$ cm, $Re_{\delta^*} = 330$.

approaching from upstream to be deflected laterally outward and down towards the surface. In plan-view visualizations of the present study, high-speed inflow regions were always observed to flank the low-speed outflow regions created by the counter-rotating legs of a hairpin vortex – an apparent result of continuity considerations.

A typical hairpin-vortex formation process, as viewed on the symmetry plane using a vertical hydrogen-bubble wire, is shown sequentially in figure 6. The undisturbed flow in figure 6(*a*) indicates a laminar velocity profile near the wall (0.06 s after the initiation of the injection). During the injection process, flow is retarded near the wall, as evidenced by the thinning and deformation of the hydrogen-bubble lines in figure 6(*b*). As time increases, the flow is further retarded near the wall (the lines move closer together), developing a pronounced local inflection-type profile (figure 6*d*). Shortly thereafter, the vortex head begins to form (figure 6*e*, *f*) as the injected flow penetrates outward. The presence of the vortex head is evidenced by the curvature of the hydrogen-bubble lines towards the middle of the vortex head as indicated in figure 6(*g*). The flow immediately above the vortex head (labelled A in figure 6*g*) accelerates with respect to the mean (increased spacing of the material lines), whereas the flow behind the vortex head at B decelerates. Following formation, the hairpin-vortex structure begins to elongate and move outward away from the wall as it advects out of the field of view (figure 6*h*).

From an assessment of the visualization studies, the following observations regarding the hairpin-vortex formation process are made: (*a*) the injection process locally decelerates the streamwise flow, causing the development of an inflectional velocity region, from which the hairpin head develops, (*b*) the injection process both introduces new vorticity and perturbs the existing boundary-layer vorticity, (*c*) deformation and stretching of the perturbed vorticity leads to the eventual formation of the hairpin vortex.

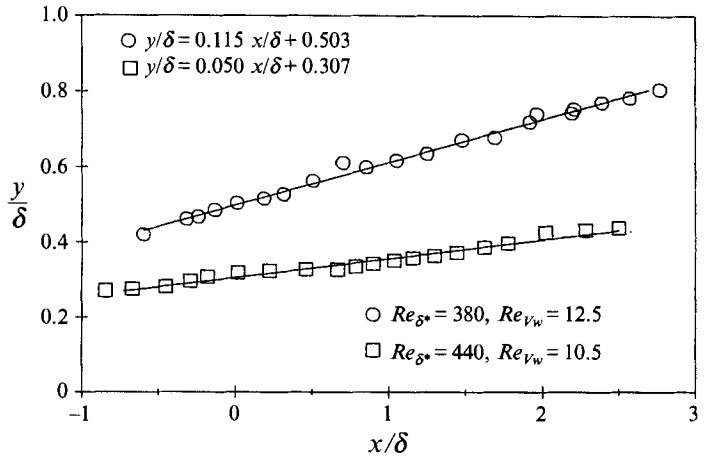

FIGURE 7. Spatial displacement of the vortex head during formation, in the vicinity of the injection slot, $-1 < x/\delta < 3$.

3.4. *Kinematics of the hairpin vortex*

Visualization studies using dye-marked injection fluid and a vertical hydrogen-bubble wire over a broad range of injection parameters were done to establish: (i) the elapsed time for the formation of a vortex head from the initiation of the injection, and (ii) the downstream distance required for the formation of a complete vortex head. It was qualitatively observed that the hairpin-vortex head forms rather quickly after the initiation of the injection (usually within one to three times the injection stroke time).

Additionally, the visualization results generally indicate that for $Re_{\delta^*} > 255$ hairpin vortices form completely within the boundary layer and within $2 < x/\delta < 4$ downstream of the leading edge of the injection slot. As the plate Reynolds number is increased, the formation location moves downstream and closer to the edge of the laminar boundary layer.

Following formation, a hairpin structure will move away from the wall and advect downstream. Figure 7 illustrates the spatial motion of the vortex head for two different injection parameters and Reynolds numbers ($Re_{V_W} = 12.5$, $Re_{\delta^*} = 380$; and $Re_{V_W} = 10.5$, $Re_{\delta^*} = 440$). Note that for the region shown, an essentially linear outward movement of the vortex head is observed; as the vortices move farther downstream, the head moves outside the edge of the boundary layer and the outward motion ceases. For the two cases compared in figure 7, the hairpin vortex head for $Re_{\delta^*} = 380$ moves along a steeper path than for $Re_{\delta^*} = 440$, possibly because of the higher injection rates required.

Characteristically, past studies of coherent structure in turbulent boundary layers (e.g. Theodorsen 1952; Head & Bandyopadhyay 1981) have placed great stock in hypothesized hairpin-vortex structures having a characteristic angle of 45° (the angle of maximum strain) to the bounding surface. However, this angle clearly must vary as the flow structure approaches the wall, or penetrates beyond the high-shear region of the boundary layer, where the mean stretching angle will diverge from 45°. To examine these projected geometric changes during the hairpin formation, the angles described by the vortex legs and head during the formation process were examined as a function of Reynolds numbers and injection parameters. In general, the designation of a 'characteristic' angle was found to be relatively arbitrary owing to the curvature of the leg/head geometry. Repeated observations suggested that one could define four

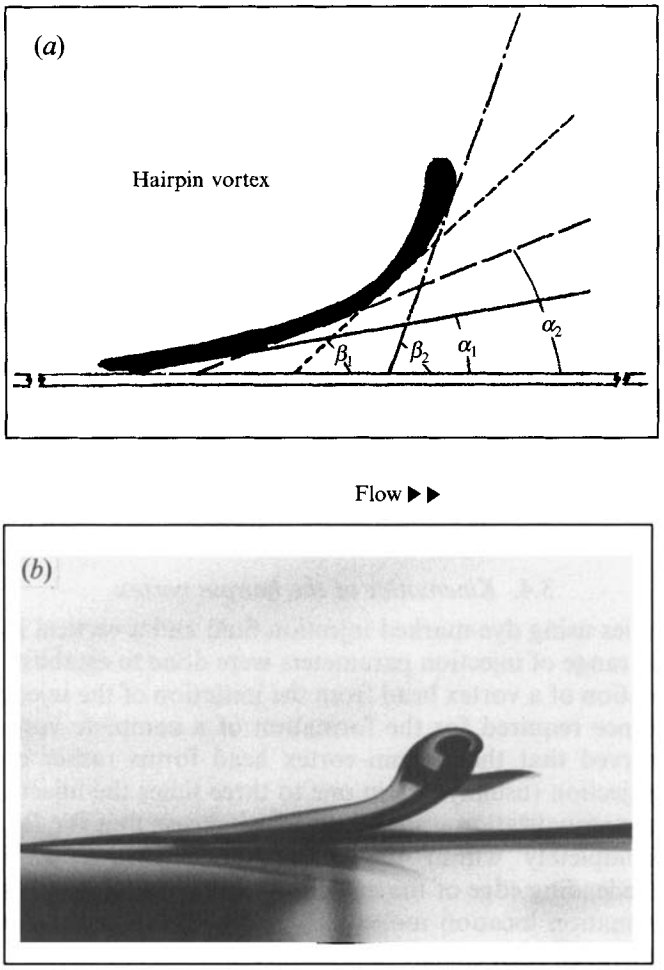

FIGURE 8. Angles associated with a hairpin vortex during formation. (*a*) Schematic diagram illustrating the four characteristic angles identified with a single hairpin vortex; (*b*) a typical side-view dye picture used to establish the vortex angles.

characteristic angles for the legs and the head of the vortex, as shown schematically in figure 8. Angles α_1 and α_2 characterize the angles of the legs of the vortex, and angles β_1 and β_2 characterize the head of the hairpin vortex; a typical dye visualization used to establish these angles is shown in figure 8(*b*).

The results of the geometric evaluation were tabulated for a range of displacement and injection Reynolds numbers (see Haidari 1990). The tabulations generally suggest that the geometric characteristics of a hairpin vortex are not significantly affected by changes in plate Reynolds number. During the formation process, hairpin-vortex varies generally as follows:

$15° > \alpha_1 > 6°$, the upstream portion of the legs;

$14° < \alpha_2 < 32°$, the downstream portions of the legs;

$27° < \beta_1 < 54°$, the section connecting the vortex legs and head;

$48° < \beta_2 < 67°$, vortex head.

During the formation process, the hairpin vortex continually moves away from, and at ever-increasing angles to, the surface, with the exception of the upstream extensions of the legs, which move towards the wall at ever-decreasing angles. Note that the section which defines the β_1 angle is observed to vary from 27° to 54°, which suggests that β_1 is the flow structure angle most often characterized in flow structure studies of turbulent boundary layers and turbulent spots. For example Head & Bandyopadhyay (1981) report that the dominant flow structures they detected had a characteristic angle of 45°; and Matsui (1980) in a study of a natural turbulent spot reported a characteristic angle of 38°.

4. A single decaying hairpin vortex

An extensive investigation of the downstream development of single hairpin vortices suggests that a hairpin vortex can be classified as either a decaying or growing vortex. A decaying vortex displays little, if any, effect on near-wall surface fluid, with the initial vorticity of the hairpin vortex diffusing due to viscosity; in contrast, a growing vortex interacts strongly with near-wall surface fluid, resulting in strong fluid eruptions from the surface which stimulate the generation of new vortices in its wake. In this section, results are presented which illustrate some of the characteristics of single decaying hairpin vortices. Section 5 presents results for growing vortices.

4.1. *Velocity patterns*

The streamwise velocity induced by a moving hairpin was measured with a single-element hot film, on both the symmetry and off-axis planes. Measurements were carried out at three streamwise locations and for a number of off-axis locations. At each measurement location, measurements were taken at selected heights ranging from adjacent to the surface to the top of the hairpin vortex.

The injected fluid was marked with dye to enable visualization of single hairpin vortices as they passed the hot-film sensor. Figure 9 is a typical split-screen sequence of simultaneous dye visualization and hot-film measurement. The passage of a single hairpin vortex (generated for $Re_{\delta^*} = 330$, and $Re_{Vw} = 11.2$) across the hot-film probe is illustrated in figure 9(*a–g*). The top part of figure 9 is the corresponding oscilloscope display of the velocity signal. Figure 9 shows that as the single hairpin vortex approaches the sensor (figure 9*b*), the velocity begins to decrease, continuing as the vortex head passes the sensor (figures 9*c* and 9*d*). By figure 9(*d*), the middle of the hairpin-vortex head has passed the probe and the velocity begins to rapidly increase, which continues through figure 9(*e*). As the hairpin-vortex head passes the sensor, the velocity again decreases, with a recovery of the velocity signal back to the local mean level by figure 9(*g*). Consistent with the side-view hydrogen-bubble visualization shown in figure 6, the passage of a single hairpin vortex results in a flow deceleration followed immediately by a strong acceleration of the flow.

In figure 10 velocity traces similar to those shown in figure 9 are phase-referenced on the peak signal and superimposed. This process in effect illustrates the temporal behaviour of the streamwise velocity as if it were detected with an inclined rake of hot-film probes tilted at an angle such that all the probes simultaneously detect the peak local velocity (highest probe most downstream). The relative vertical detection locations are illustrated in figure 10 with reference to the single hairpin vortex.

Figure 10 suggests that the hairpin vortex head produces the most coherent part of the signal. The amplitudes of the signals presented for the three streamwise locations of figure 10 appear to be the highest close to the slot ($X_{\text{probe}} = 0$) and during the

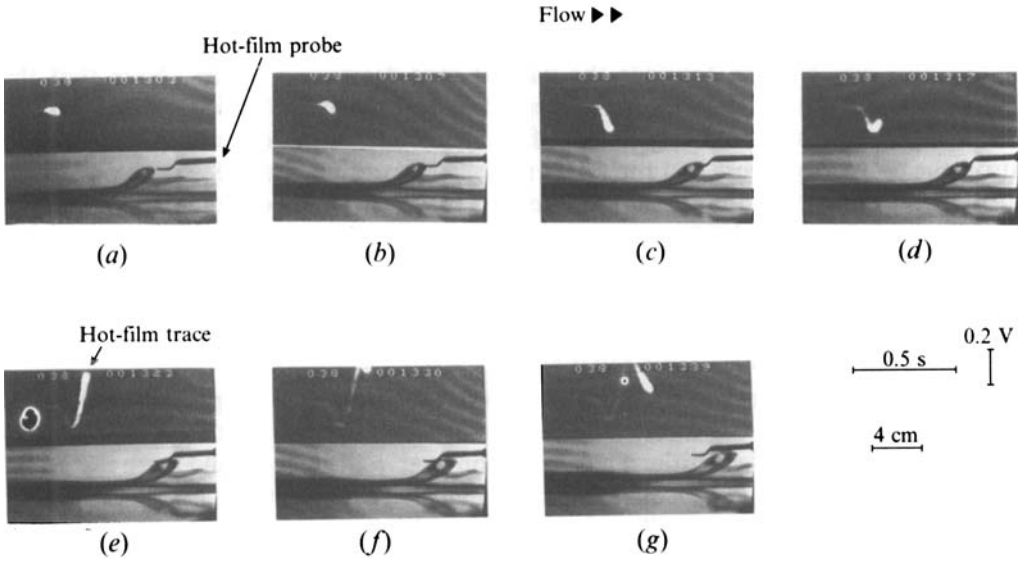

FIGURE 9. Combined split-screen dye visualization and hot-film anemometry sequence illustrating the streamwise component of velocity induced by a hairpin vortex. $x_{\text{probe}} = 4.0$ cm, $y_{\text{probe}} = 0.5$ cm. $Re_{\delta^*} = 330$, $Re_{Vw} = 11.20$, $U_\infty \approx 8.8$ cm s^{-1}, $\delta^* = 0.4$ cm.

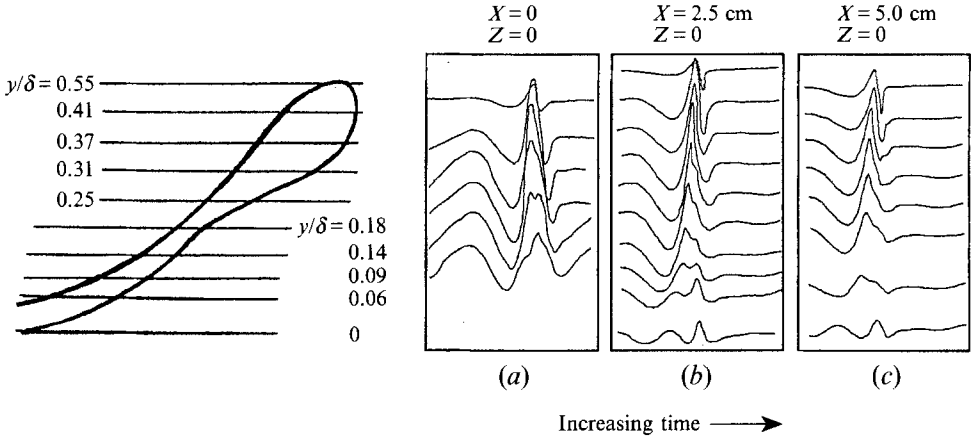

FIGURE 10. Streamwise velocity due to the passage of a single hairpin vortex measured using hot-film anemometry at three streamwise stations and a series of vertical locations on the plane of symmetry of the vortex. $Re_{\delta^*} = 330$, $Re_{Vw} = 11.20$.

formation process. As shown, the vortex head induces an initial deceleration followed by a subsequent acceleration in the streamwise flow. This velocity behaviour is very similar to the velocity patterns characterized as 'burst' signatures in turbulent boundary layers (e.g. Bogard & Tiederman 1986). Note that as the velocity probe is moved close to the wall, where flow is predominantly influenced by the counter-rotating legs of the vortex, the coherency and amplitude of the signals in figure 10 are reduced.

Spanwise flow behaviour near the injection slot was examined at selected lateral locations off the symmetry plane. Superimposed velocity traces similar to figure 10 are shown in figure 11 for five spanwise locations at $X_{\text{probe}} = 0$. At a glance, it is clear that

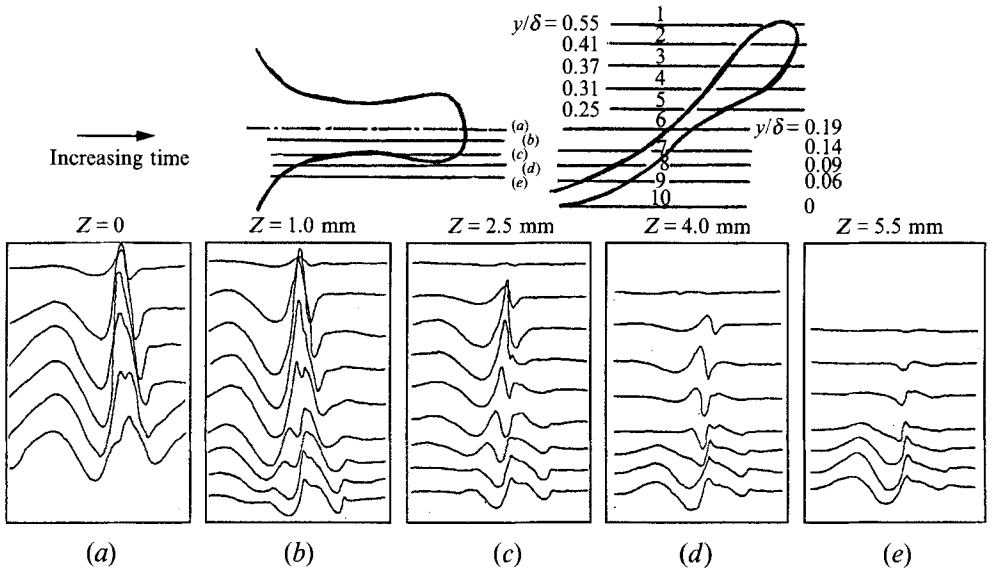

FIGURE 11. Streamwise velocity traces due to the passage of a single hairpin vortex. Taken in five lateral planes at $x = 0$. Signals are phrase-referenced from a single hot-film probe output. $Re_{\delta^*} = 330$, $Re_{Vw} = 11.20$, $U_0 \approx 8.8$ cm s^{-1}, $\delta^* = 0.4$ cm.

the hairpin velocity variations are strongest near the symmetry plane. Figure 11(*b*), with the hot-film probe located only 1 mm off the symmetry plane, is essentially similar to figure 11(*a*); at $Z = 2.5$ mm (figure 11*c*), the strong variations due to the vortex head are diminished. However, the velocity signals near the wall appear unaffected, suggesting that velocity signals close to the wall are predominantly due to the velocity induced by the legs of the vortex. At subsequent locations off the symmetry plane (figures 11*d* and 11*e*), the velocity induced by the vortex is largely minimized, with the largest velocity excursions occurring near the surface, owing to interaction of the leg of the vortex with the surface.

There is substantial similarity between the traces shown in figures 10 and 11 with comparable results from a study by Head & Bandyopadhyay (1981) associated with the identification of hairpin vortices in a turbulent spot. The similarity of the velocity traces provides substantial support for the hypothesis of Head & Bandyopadhyay (1981) for the presence of hairpin vortices in a turbulent spot. In addition, examination of the conditional average of the streamwise velocity at $y^+ = 12$ in a turbulent boundary layer, as obtained by Blackwelder (1978), suggests a decelerating/accelerating behaviour very similar to that observed in figures 10 and 11.

4.2. *End-view visualization*

Laser-light-sheet illumination was employed in conjunction with a horizontal hydrogen-bubble wire for end-view visualization of single hairpin vortices. Figure 12 is an end-view sequence of a single hairpin vortex visualized using laser-sheet illumination. The hydrogen-bubble wire was located transverse to the flow, 2 mm above the wall and 7.5 cm upstream of the laser-light sheet. Single hairpin vortices were visualized using dye in the injection fluid. The outer extent of the hairpin-vortex head is faintly visible and is indicated by the arrow in figure 12(*a*); note that the single hairpin vortex has not yet reached the laser sheet in this figure. As the vortex head passes in proximity to the hydrogen-bubble wire, the bubbles are entrained by the

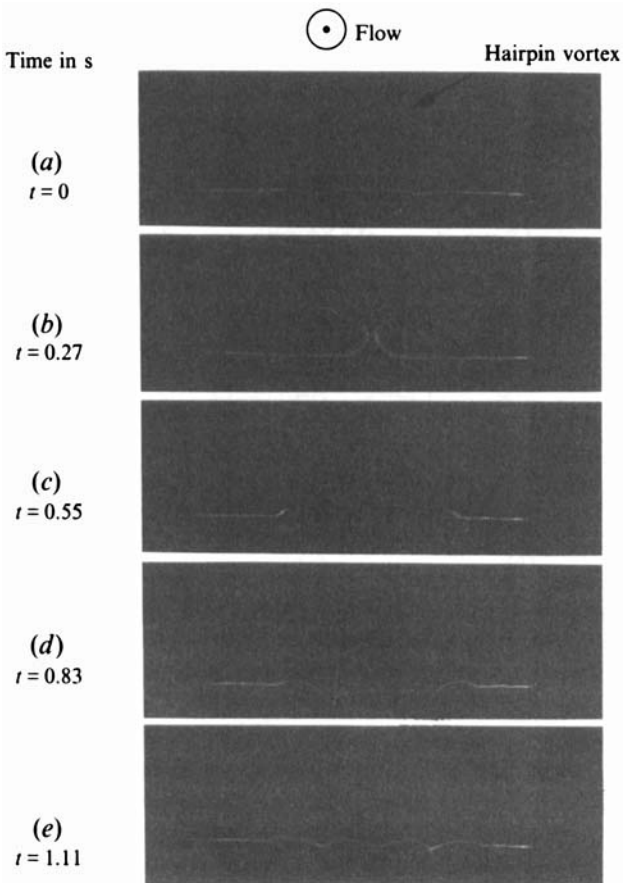

FIGURE 12. End view of combined dye and hydrogen-bubble visualization of a single hairpin vortex using a laser light sheet. $Re_{\delta^*} = 340$, $Re_{VW} = 13.35$, $x_{\text{wire}} = 1$ cm, $y_{\text{wire}} = 0.2$ cm, and $x_{\text{light}} = 8.5$ cm.

vortex legs, appearing as 'wave-like' patterns as they pass through the laser sheet (figure 12*b*). Continued passage of the vortex through the laser sheet shows that the legs move closer to the wall and farther apart. In figure 12(*c*) the centres of the counter-rotating legs appear just above the wire; note the lateral extent of the vortex, and the symmetry of the outboard structures. By figure 12(*d*), the centres of the vortex legs have moved lower, to essentially the level of the hydrogen-bubble wire, very close to the wall. As the structure moves farther downstream, laminar flow begins to re-establish itself (figure 12*e*), although the vestiges of the flow induced by the extended weakened legs can still be seen.

5. Growth of a single hairpin vortex

In this section the downstream growth processes responsible for the evolution of a single hairpin vortex into a turbulent-spot-like structure are presented. The generation of a turbulent spot by local perturbation of a laminar boundary layer has been the subject of a number of studies, both experimental (e.g. Coles & Barker 1975; Wygnanski 1978) as well as analytical (e.g. Kral & Fasel 1989). Several studies have attempted to investigate the flow structure within a turbulent spot (Perry, Lim & Teh 1981; Sankaran, Sikolov & Antonia 1988), and suggest that a spot is an agglomeration

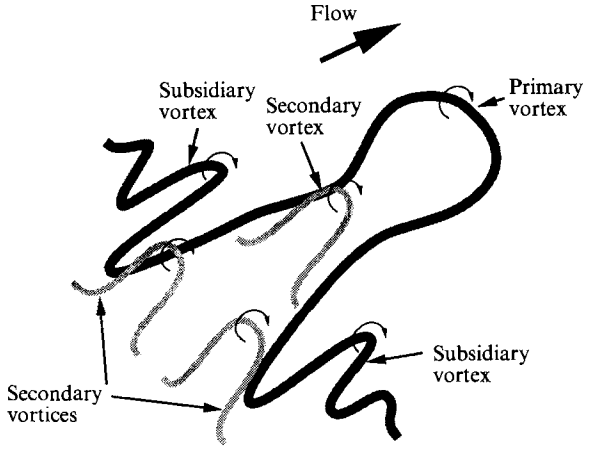

FIGURE 13. Schematic of the hierarchy of observed hairpin-like vortices.

of smaller flow structures, of which hairpin vortices are suggested as models. However, the process of development of such internal flow structures has never been demonstrated. The following section provides results which illustrate that an initial hairpin vortex can grow to a turbulent-spot structure through systematic generation of new vortices.

5.1. *Initial growth of a single hairpin vortex*

The hairpin vortices considered in the present section are strongly interactive, demonstrating remarkable reproductive characteristics which cause growth of the structure by development of additional hairpin vortices, both laterally and in their wake. Figure 13 is a schematic illustrating the terminology used to describe the hairpin vortex growth process. The initial hairpin vortex, which develops as the result of the injection process, is referred to as the primary vortex (P). Vortices which form as the result of the interaction of the primary vortex (either the vortex head or the legs) with surface fluid are considered to be secondary vortices (S). A second group of vortices which normally form outboard of the primary vortex are termed subsidiary vortices (SU) and, as indicated in figure 13, substantially trail the primary-vortex head; subsidiary vortices are believed to be associated with the inviscid deformation of the vortex lines comprising the primary vortex (see Smith *et al.* 1991).

5.1.1. *Flow patterns created by a hairpin vortex*

The results presented in this section are either direct hydrogen-bubble patterns or schematic interpretations which have been deduced from hydrogen-bubble visualization data obtained over a wide range of flow conditions. Viewing the present results in both real time and slow motion revealed that the flow patterns generated by hairpin vortices are both distinctive and very repeatable. In the absence of a dynamic means to present the visualization results, plan-view photographs with accompanying schematic interpretations are shown in figures 14 and 15 to illustrate the type of characteristic patterns generated by different parts of a hairpin vortex structure. Since hydrogen bubbles mark the most active regions of the flow being visualized, the patterns observed during the examination of a dynamic three-dimensional hairpin flow structure are sensitive to the hydrogen-bubble-wire location. Different flow patterns are observed depending on which portion of the flow structure is locally active relative to the wire location.

Figure 14, obtained with the hydrogen bubble wire at $x = 1$ cm, shows the initial and

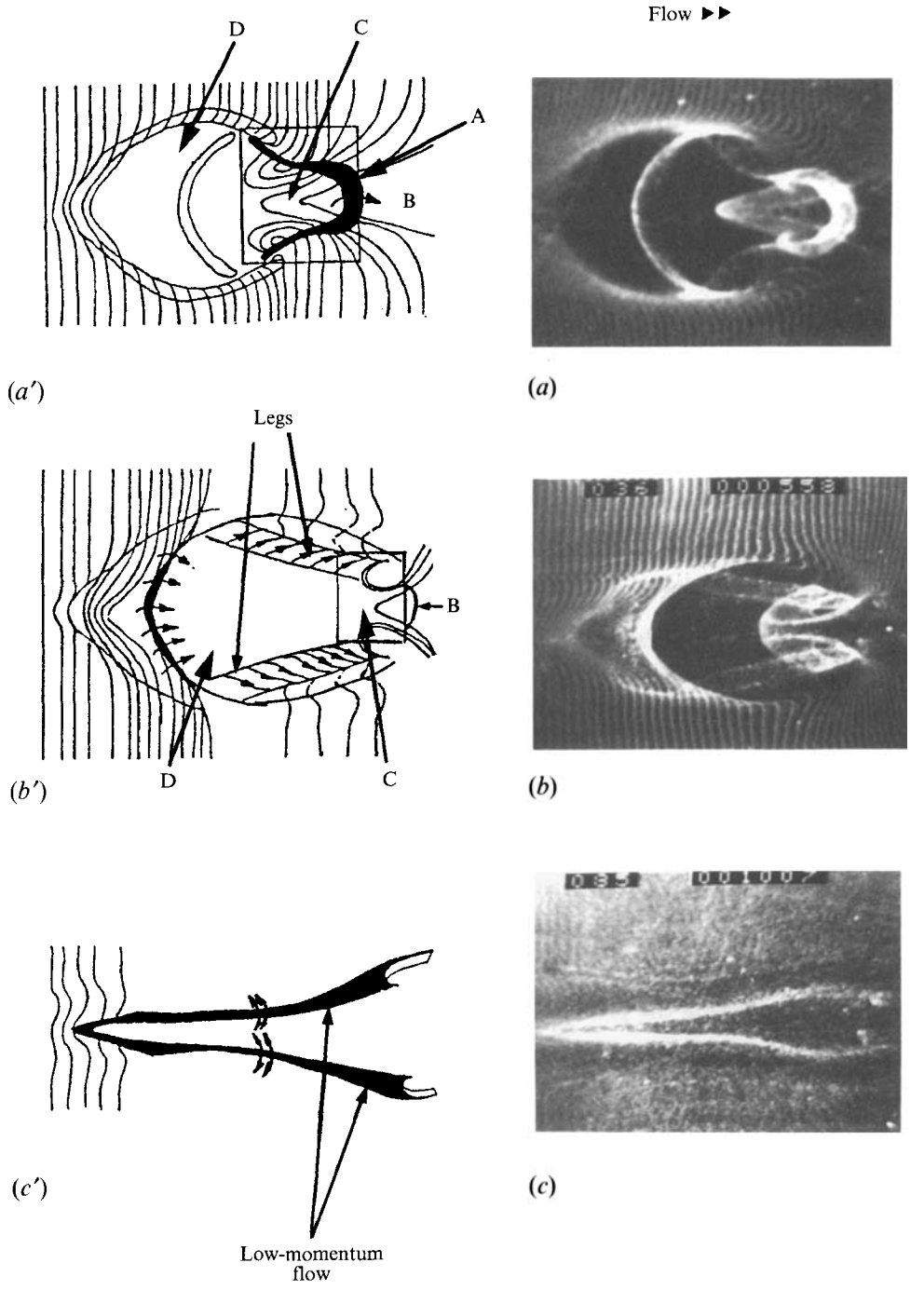

FIGURE 14. The dominant flow patterns associated with a single hairpin vortex immediately after formation. $Re_{\delta^*} = 440$, $x_{\text{wire}} = 1.0$ cm: (a, a') $y_{\text{wire}} = 0.63$ cm, (b, b') $y_{\text{wire}} = 0.51$ cm, (c, c') $y_{\text{wire}} = 0.127$ cm, $U_0 = 13$ cm s^{-1}, $\delta^* = 0.34$ cm.

most characteristic flow pattern for a single hairpin vortex. In figure 14(*a*) the head of the vortex has just passed through the bubble sheet, generated at 0.63 cm above the surface. The vortex head is the dark region in figure 14(*a'*) and is labelled A, with the sense of rotation of the vortex head as indicated. The rotation of the vortex head creates a radial pressure gradient which causes the hydrogen bubbles to concentrate within the head, creating the bright Ω shape in figure 14(*a*); the associated kinematics of the head are indicated in three regions labelled B, C, and D. As the hairpin vortex rises through the bubble sheet, the flow in region B undergoes a strong deceleration, such that flow is drawn beneath the head, forming the bright triangular region C. Region D is devoid of hydrogen bubbles, with the bubbles from region D either entrained into the vortex head as the vortex passes through the bubble sheet, or transported upstream of this region. Basically, the rotation of the vortex head and the counter-rotating legs of the hairpin vortex yield a saddle point in region D.

With the hydrogen bubble wire lowered to 0.51 cm, the streamwise, counter-rotating legs of the hairpin vortex become visible. The regions labelled B, C, and D in figure 14(*b'*) are essentially the same as those pointed out in figure 14(*a'*). Figures 14(*a*) and 14(*b*) are the most characteristic patterns indicative of a single hairpin vortex; patterns similar to those shown in figures 14(*a*) and 14(*b*) could always be observed whenever a hairpin vortex was present. The patterns similar to figure 14(*b*) are considered to be a 'turbulent pocket', because of the 'pocket' of unmarked fluid associated with these patterns and the characteristic U shape of the region, essentially identical to the turbulent 'pocket' structures described by Falco (1991).

As the hydrogen-bubble wire is lowered towards the wall, the influence of the vortex head on the bubble sheet is reduced. In figure 14(*c*) the hydrogen bubble wire is located 0.127 cm above the wall, illustrating the pattern created by the interaction between the counter-rotating legs and the surface fluid. The two bright narrow streamwise regions appearing in figure 14(*c*) are concentrated hydrogen bubbles, indicative of low-momentum upwellings of near-wall fluid. These low-momentum regions, as indicated in figure 14(*c'*), are observed to oscillate and sway in the spanwise directions, in a manner remarkably similar to the low-speed streaks of a turbulent boundary layer (Kline *et al.* 1967; Smith & Metzler 1983).

Figure 15 illustrates several typical flow patterns which appear when the hydrogen-bubble wire is moved downstream to $x = 5.0$ cm. At this location the head of the vortex is centred at a height of $y = 0.95$ cm, about 25% higher than the height of the vortex head in figure 14(*a*). In figure 15(*a*), the effects of the counter-rotating legs of the vortex are visible in the plane of the bubble sheet, and are indicated in the schematic of figure 15(*a'*). Regions B and D correspond to similar regions shown in figure 14(*a*) and reveal similar kinematics. The dotted lines indicate the boundaries between the flow affected by the counter-rotating legs of the vortex and the undisturbed flow. The narrow bright region of concentrated hydrogen bubbles labelled F in the schematic is observed to form in the plane of symmetry of the structure, and extends down to the boundary surface.

In figure 15(*b*), with the wire closer to the wall, the counter-rotating legs of the hairpin vortex becomes more apparent (indicated by the arrows). The bright regions outboard of the primary legs G are regions of lateral outward-directed flow, corresponding to the dotted lines of figure 15(*a'*), and indicate the boundary between the region affected by the interaction of the counter-rotating legs of the hairpin and the surrounding laminar flow. Since the vortex legs move away from each other as they move closer to the surface, the turbulent pocket-like region D appears larger and closer to the wall. Upstream of region D, a secondary hairpin vortex begins to form. Note in

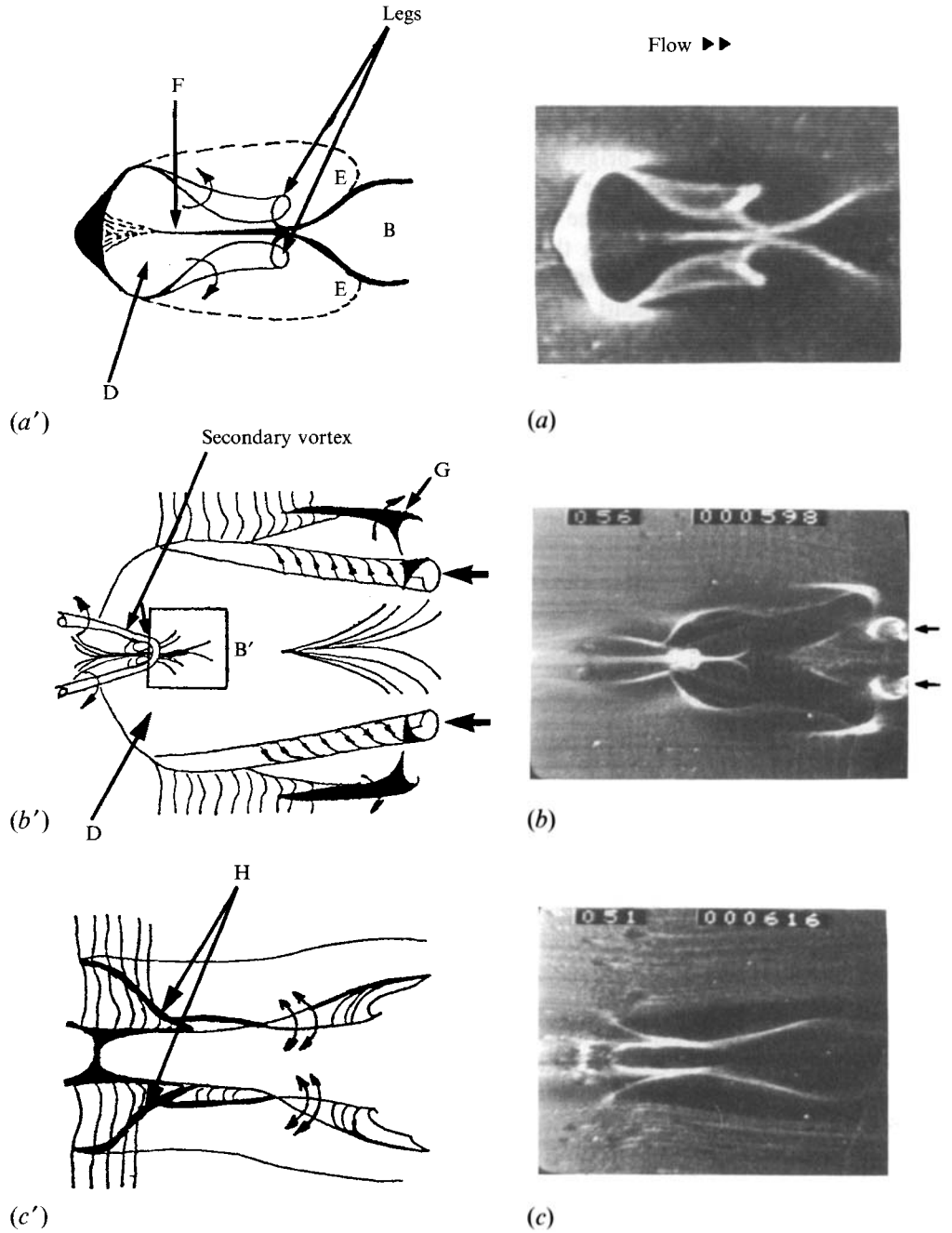

FIGURE 15. Dominant flow patterns generated by a developing single hairpin vortex. $Re_{\delta^*} = 440$, $x_{\text{wire}} = 5.0$ cm: (*a*, *a*′) $y_{\text{wire}} = 0.76$ cm, (*b*, *b*′) $y_{\text{wire}} = 0.63$ cm, (*c*, *c*′) $y_{\text{wire}} = 0.127$ cm.

figure 15(*b*′) the presence of a retarded flow region labelled B′ appearing just downstream of the secondary vortex head (similar to region B of figures 14*a*′ and 14*b*′).

Figure 15(*c*) shows the effect of the developing hairpin vortex on near-wall fluid. The bright narrow regions of figure 15(*c*) are low-momentum streak-like regions created by the strong interaction of the legs of the primary hairpin with fluid immediately adjacent to the boundary. Two noticeable differences between figure 15(*c*) and the same region

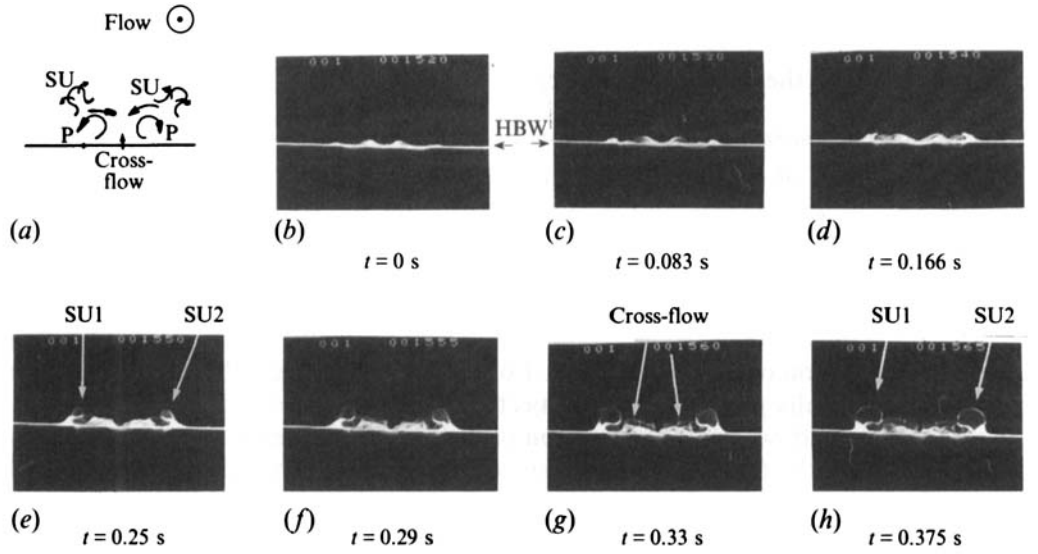

FIGURE 16. Formation of subsidiary vortices, visualized in end view. $Re_{\delta^*} = 440$, $x_{\text{wire}} = 20$ cm, $y_{\text{wire}} = 0.35$ cm.

shown in figure 14(*c*) are: (*a*) a clear separation of the two low-momentum regions, and (*b*) the presence of the distinct ridges labelled H in figure 15(*c'*), which appear to be due to the development of secondary hairpin vortices. The low-momentum regions of figure 15(*c*) are again observed to oscillate in the cross-stream plane, similar to the behaviour of turbulent low-speed streaks.

The hydrogen-bubble patterns shown in figures 14 and 15 are very typical of the patterns associated with the passage of a single hairpin vortex, and are so ubiquitous that they can serve as templates for identification of the presence of hairpin vortices as the vortex grows to a turbulent spot (§5.2).

5.1.2. *Subsidiary hairpin-vortex structure*

The formation of the subsidiary vortices (see figure 13), appears to be the result of the inviscid deformation of the collective vortex lines comprising the primary vortex. As discussed in §1.2, three-dimensional Biot–Savart calculations by Hon & Walker (1987) and Smith *et al.* (1991) of the motion and deformation of a single vortex line indicate the development of subsidiary vortices by lateral inviscid deformation. Hon & Walker show that when a perturbed line vortex is subjected to a uniform shear, the initial distortion will amplify to form a hairpin vortex. Additional spanwise deformation induced by Biot–Savart interaction gives rise to new hairpin vortices which develop outboard of the symmetry plane of the initial hairpin vortex. Smith *et al.* (1991) further illustrates that the presence of an asymmetric deformation results in a non-symmetric amplification process, but that subsidiary vortices still form, indicating that the generation process is generic, and not dependent on flow symmetry.

An end-view visualization sequence shown in figure 16 illustrates the presence of the subsidiary vortices. A horizontal hydrogen-bubble wire, positioned to isolate the head of the subsidiary vortices, provides a chronological view of the different parts of the flow disturbance as they pass through the focal plane of the camera. The overall flow behaviour is represented schematically in figure 16(*a*), followed by the related visualization pictures. The initial hydrogen-bubble deformation in figure 16(*b*, *c*) is due to the effect of the primary single hairpin vortex. Subsidiary vortices (SU1 and SU2)

become apparent by figure 16(*d*), and can be clearly recognized by figure 16(*f*). The subsidiary vortices grow very rapidly and are influenced by the lateral motion of the fluid generated by the primary-vortex legs.

5.1.3. *Secondary hairpin-vortex structure*

The formation of secondary hairpin vortices (see figure 13) is the result of inviscid/viscous interactions between outer-layer fluid and sharp eruptions of surface fluid caused by the interaction of the primary hairpin vortex with the surface.

The process of formation of a secondary vortex is similar to the formation process for the primary vortex. In §3.2 it was illustrated that a lift-up of low-momentum fluid initiates three-dimensional deformation of spanwise vorticity, which eventually gives rise to the formation of a hairpin vortex. For the primary vortex, the low-momentum region was artificially generated by the injection process. However, secondary vortices are created by the downstream interaction of the primary vortex with surface fluid. A detailed model of the formation of hairpin vortices based on the current experimental data and concurrent analytical/numerical investigation of hairpin vortex growth is presented elsewhere (Smith *et al.* 1991). In this section, visualization results supporting that model are presented.

The present results, in conjunction with the experimental observation of Acarlar & Smith (1987*a*, *b*), and analytical/numerical studies of Hon & Walker (1987) and Peridier & Walker (1989), allow the following physical model of secondary vortex formation to be hypothesized (see also Smith *et al.* 1991). Initially, the action of the primary hairpin vortex imposes a locally transient three-dimensional adverse pressure gradient on the surface, consisting of (i) a streamwise gradient, due to the action of the vortex head, and (ii) regions of spanwise adverse pressure gradient generated by the action of the counter-rotating legs. If the primary vortex (*a*) is sufficiently strong, and (*b*) remains in proximity to the surface for a sufficient time period, it will initiate a localized viscous growth of wall fluid, which will rapidly focus and 'erupt' from the surface. This spire of fluid will subsequently interact with the outer flow in what is termed an inviscid–viscous interaction (Van Dommelen & Cowley 1990; Periodier *et al.* 1991). This interaction appears to be the necessary step which results in the formation of secondary hairpin-vortex structures.

Figure 17 is a sequence of plan-view photographs, which demonstrate the development of secondary vortices. In figure 17(*a*), the parent hairpin vortex has arrived in the vicinity of the field of view, with the hairpin head well above the bubble sheet at approximately the right-hand edge of figure 17(*a*). The clear regions A are where the legs of the hairpin pass through the plane of the bubble sheet. The vortex-induced flow sweeps the bubbles away, as discussed in §5.1.1, and the clear zones A effectively mark the local outline of the cores of the vortex legs. At the next instant (figure 17*b*), the parent hairpin vortex has moved to the right, and the outline of a small eruptive region at location B is just visible. The formation of region B marks the beginning of an eruptive event which leads to formation of a new hairpin vortex (see Van Dommelen & Cowley 1990; Smith *et al.* 1991). With passage of time the low-momentum fluid at B moves rapidly outward and, as may be inferred from figure 17(*c–e*), a process of roll-up and formation of a new vortex occurs. Additionally, the beginning of a similar process of surface eruption and roll-up near the trailing vortex legs develops at C in figure 17(*d*). As may be observed in figure 17(*f–h*), three new hairpin vortices (one on the symmetry plane and one adjacent to each leg of the hairpin) have been generated by interactions of the primary hairpin vortex with the surface flow, and continue to grow and move farther from the wall.

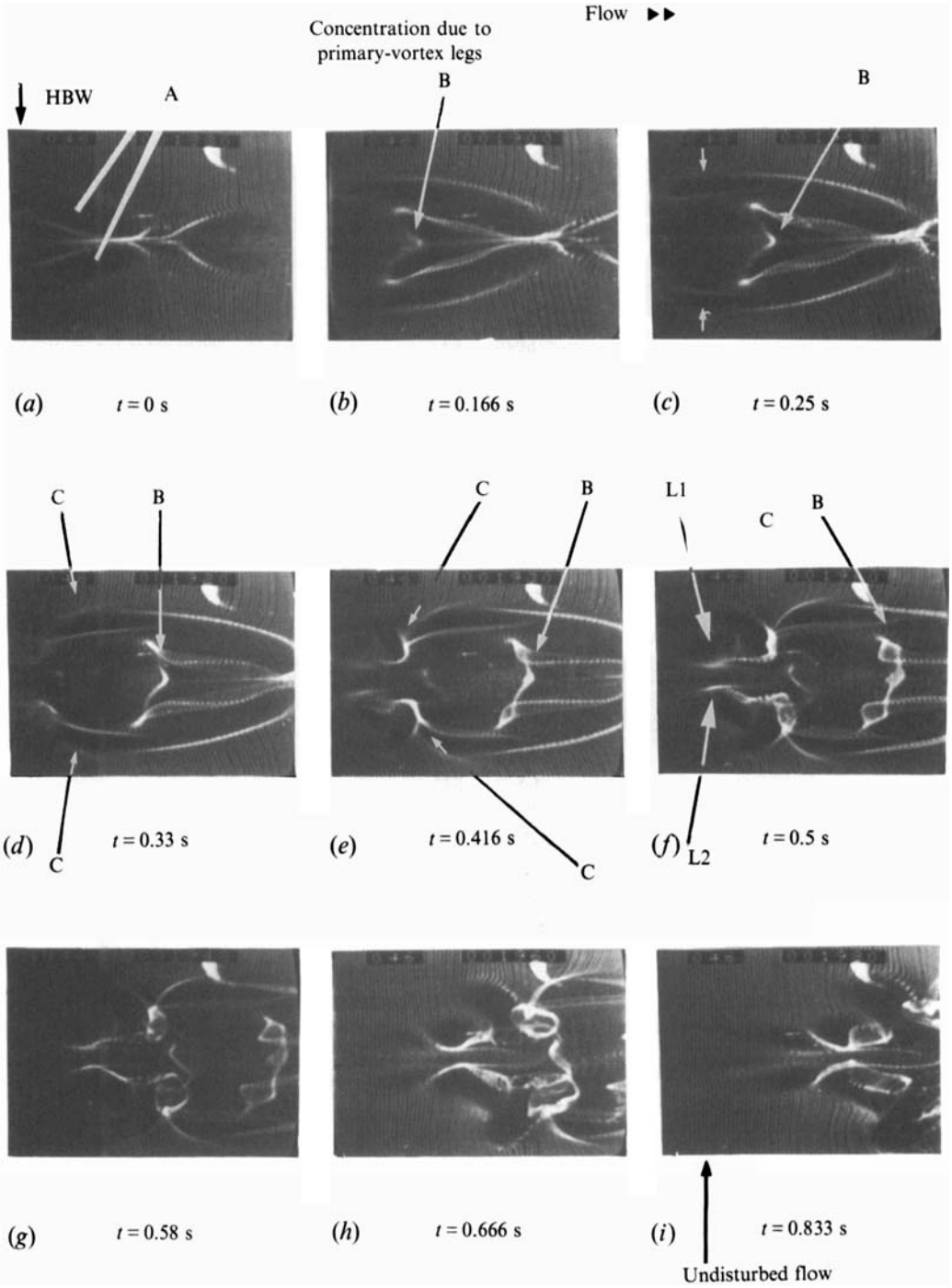

FIGURE 17. Plan-view hydrogen-bubble-wire visualization sequence illustrating the development of secondary vortices near the surface as a primary hairpin vortex passes a fixed streamwise location. HBW denotes the position of the hydrogen-bubble wire, A the location of the trailing legs of the primary vortex, B the development of a secondary vortex behind head of the primary, C the development of secondary vortices adjacent to the legs of the primary vortex, and L1, L2 the legs nearest the symmetry plane for the secondary vortices indicated by C. $Re_{\delta^*} = 440$.

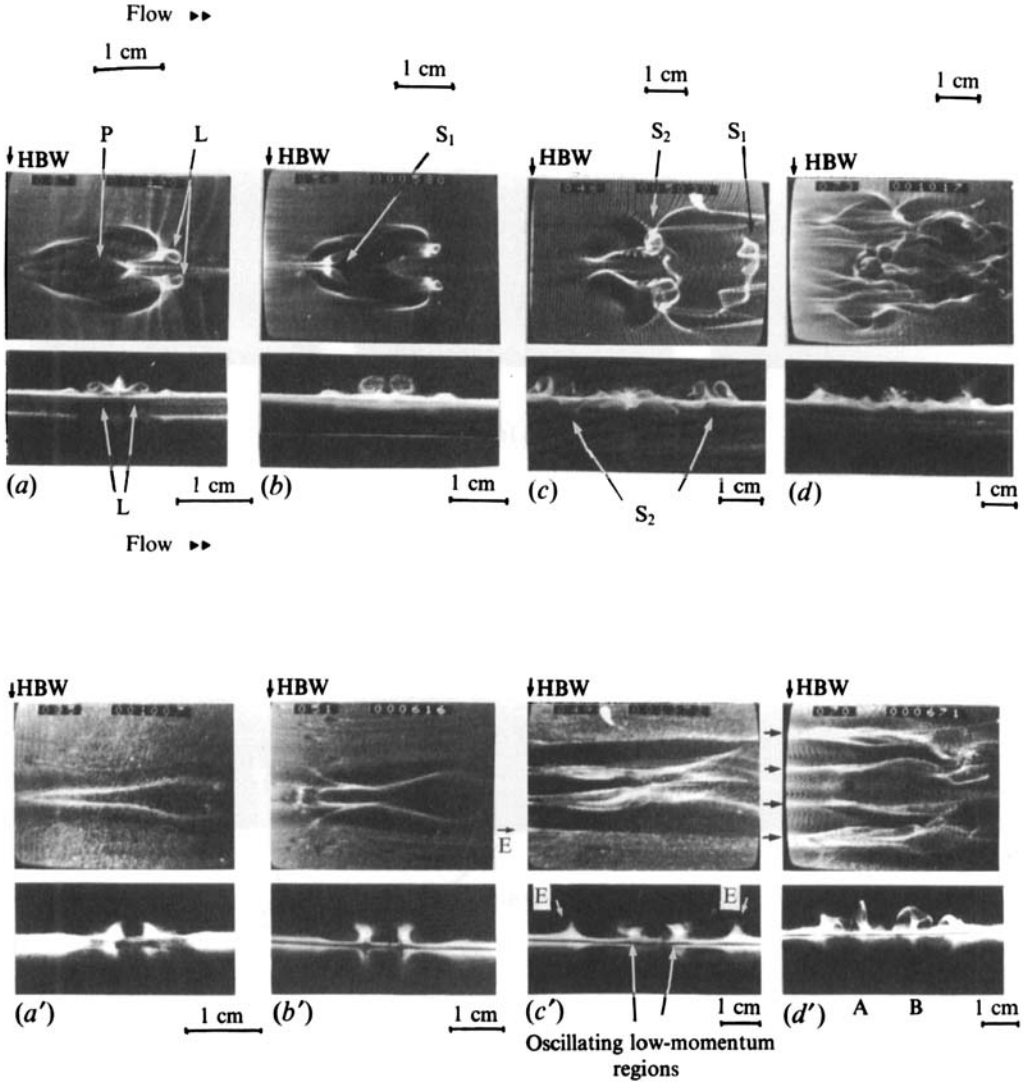

FIGURE 18. Plan-end view hydrogen-bubble patterns generated by the passage of a developing hairpin structure. Dual-level pictures: *a–d* HBW located at $y/\delta = 0.4$, with (*a*) $x/\delta = 1$, (*b*) $x/\delta = 5$, (*c*) $x/\delta = 10$, (*d*) $x/\delta = 30$. In (*a′–d′*) HBW located at $y/\delta = 0.1$ and identical streamwise locations. $Re_{\delta^*} = 440$.

A closer examination of figure 17 reveals an interesting difference between the process that occurs behind the parent vortex head and the process adjacent to the trailing legs. The roll-up B that occurs behind the vortex head occurs principally in the streamwise direction and yields a new secondary hairpin of the same orientation as that of the parent hairpin vortex. On the other hand, the eruptive process that gives rise to the formation of the secondary hairpin vortices C near the trailing legs occurs along ridges that are skewed inward towards the plane of the symmetry of the parent hairpin vortex.

5.2. *Development to a turbulent spot*

The process of vortex regeneration, both laterally and in the wake of the primary vortex, leads to the continued growth and development of the original hairpin vortex into a turbulent spot structure. To examine the spot development process, extensive

hydrogen-bubble visualization and x-wire anemometry were carried out at a series of streamwise locations (Haidari 1990). Plan–end view visualizations which assist in understanding the general hairpin growth process are presented in this section.

Employing a horizontal hydrogen-bubble sheet for visualization, the downstream growth of a single hairpin-vortex structure is illustrated in a series of dual plan–end pictures in figure 18. Figure 18(*a–d*) is obtained with a hydrogen-bubble wire located parallel to the boundary at $y/\delta = 0.4$ and at streamwise distances of $x/\delta = 1$, 5, 10, and 30 respectively. Figure 18(*a′–d′*) is obtained at the same streamwise locations as figure 18(*a–d*), but with the wire located closer to the surface at $y/\delta = 0.1$. Note that in order to capture the continually expanding patterns, the field of view of the photographs in figure 18 was increased with increasing streamwise distance. A reference scale for each streamwise location is given for both the plan and end views. Note that the patterns shown in figure 18 reflect the dominant pattern observed at a particular height and location; however, no attempt has been made to temporally correlate the patterns. A detailed description of some of the more relevant aspects of the photographs follows.

Figure 18(*a*) illustrates a pattern characteristic of the passage of a single hairpin vortex, as shown previously in figure 15. Here, the counter-rotating legs lie above the plane of the bubble wire and are marked by faint tubes of bubbles (labelled L) which trail from right to left below the bubble sheet, extending down towards the plate. Figure 18(*a′*) shows the corresponding effect of the passing vortex on the wall-region fluid. The narrow bright bifurcated concentration of the bubbles in the plan-view part of figure 18(*a′*) appears in the end view as upwellings of low-speed fluid caused by the pressure-gradient-induced interaction of the legs of the vortex with fluid near the wall. It is hypothesized that these narrow concentrations are essentially the same type of flow structure as the low-speed streaks in a turbulent boundary layer.

In figure 18(*b*), the counter-rotating legs of the primary vortex are still clearly apparent in both the plan- and end-view pictures. In addition, figure 18(*b*) reveals the initiation of a secondary hairpin vortex (labelled S_1), which is just beginning to pass through the bubble sheet. As this secondary vortex develops, the head forms above the bubble sheet such that it is not visualized in the end view. The continued development of low-momentum regions near the wall is shown in figure 18(*b′*), with the narrow region shown in figure 18(*a′*) having evolved into two distinct low-momentum regions with appreciable vertical penetration.

By figure 18(*c*), the primary vortex is out of the field of view to the right, and the secondary vortex indicated in figure 18(*b*) has developed and moved away from the wall, appearing as the well-defined ridge (S_1) in figure 18(*c*). Note that the plan view of figure 18(*c*) is from the sequence of photographs presented in figure 17. Figure 18(*c*) also clearly illustrates the development of two outboard secondary vortices, labelled S_2, as discussed in §5.1.3 (figure 17).

With the appearance of the outboard secondary vortices, the flow pattern near the surface in figure 18(*c′*) begins to reflect the initiation of an additional pair of low-momentum regions. As indicated in the end view, the low-momentum regions near the centreline display a slow streamwise oscillation; the new low-speed regions E form and penetrate outward from the wall. In figure 18(*c′*), the middle two low-speed regions appear to be associated with wall interactions of the legs of both the primary and the symmetry-plane secondary vortex, while the outboard low-momentum regions appear to be associated with the wall interactions of the newly formed lateral secondary vortices.

As the flow develops downstream, the continued evolution of existing vortices and the development of new vortex structures by continued viscous–inviscid interactions

(both on the symmetry plane and laterally) results in the systematic development of a turbulent-spot flow structure that is remarkably organized and bilaterally symmetric. Figures 18(*d*) and 18(*d'*) illustrate the appearance of this spot-like structure at $x/\delta = 30$. In figure 18(*d*) the patterns and scales are similar to those observed in the near-wall region of a turbulent boundary layer, but with a greater degree of symmetry than for turbulent behaviour. This symmetry is clearly apparent in figure 18(*d'*), where the low-speed regions have developed into elongated streamwise patterns, which for all intents and purposes appear to be four very definitive turbulent-boundary-layer-type streaks (indicated by the arrows). As shown in the end view of figure 18(*d'*), these streaks oscillate laterally and penetrate substantially away from the wall, two characteristics which are universally accepted features of turbulent-boundary-layer low-speed streaks. Beyond $x/\delta = 30$ the turbulent-spot structure continues to spread, both longitudinally and laterally. The further development of this organized turbulent spot is discussed in detail in a separate publication.

6. Summary and conclusions

The present study examined the generation and growth of single hairpin vortices created by controlled injection of wall fluid from a streamwise slot with a laminar approach boundary layer. Depending on the flow parameters, one of two types of single hairpin vortices are generated by the injection process: (i) hairpin vortices which remain a single vortex, generally decaying without displaying growth of the overall flow structure, and (ii) hairpin vortices which stimulate the development of ancillary hairpin vortices, causing the overall flow structure to continually grow and expand.

The repeatable generation of hairpin vortices by the slot injection process suggests that hairpin vortices are a generic flow structure that develops from a three-dimensional perturbation of an otherwise two-dimensional shear flow. The injection process of the present study created a locally decelerated region at the wall, with an accompanying inflectional velocity profile; the head of the hairpin vortex was observed to form at the interface between the injected fluid and the displaced outer flow, in a region corresponding to the local inflection in the streamwise velocity profile. The generation of single hairpin vortices is observed to be a parametric function of both the injection and displacement Reynolds numbers, with the parameter range over which single hairpin vortices can be generated decreasing as the background shear increases.

During the formation process, the head of the vortex generally forms within the edge of the laminar boundary layer, moving upward as the hairpin vortex evolves; the shape of the hairpin develops a backwards concavity, with the angle of the most upstream portion of the legs *decreasing* from approximately 15° to 6°, and the portion of the legs extending downward from the head *increasing* from about 27° to 54°. These latter angles are the most characteristic for a single hairpin vortex, and are comparable to characteristic angles for typical flow structures in turbulent boundary layers.

A hairpin vortex regenerates new vortices by two mechanisms: (i) the lateral inviscid evolution of the initially deformed vortex lines comprising the primary hairpin vortex, creating flanking (subsidiary) hairpin vortices to either side of a primary vortex; this process initiates lateral spreading of the initial flow deformation, a process which is consistent with recent computational results; (ii) local unsteady separation effects, precipitated by the local surface pressure gradient induced by the presence of a hairpin vortex in proximity to a wall; this process creates narrow eruptions of wall-layer fluid, which subsequently interact with outer-region fluid via a viscous–inviscid interaction, generating new, secondary hairpin vortices in the wake of the primary vortex.

Many of the visualization and velocity patterns generated by hairpin vortices are markedly similar to those observed and detected in a turbulent boundary layer. The local pressure gradients imposed by the counter-rotating legs of hairpin vortices create low-momentum regions adjacent to the wall, yielding visualization patterns identical to turbulent low-speed wall-layer streaks. In the controlled conditions of the present study, each hairpin vortex generates two low-momentum regions, one associated with each leg of the primary hairpin. As new vortices develop, the number of streaks increase accordingly. These low-momentum regions are observed to be narrow regions which intermittently lift up very rapidly, penetrate well into the outer layer, and interact with the outer flow to form new hairpin-type vortices. Correspondingly, velocity traces for an advecting hairpin vortex typically illustrate a strong deceleration followed by a strong acceleration, characteristic of typical 'burst' signatures within a turbulent boundary layer.

The authors wish to thank Dr J. David A. Walker and Dr B. K. Taylor for advice and assistance, and Dr D. Rockwell for use of the laser illumination equipment. We also wish to thank the Air Force Office of Scientific Research for support of this research under grant No. AFOSR-89-0065. The continuing support of the AFOSR is gratefully acknowledged.

REFERENCES

ACARLAR, M. S. & SMITH, C. R. 1987*a* A study of hairpin vortices in a laminar boundary layer. Part 1. Hairpin vortices generated by hemisphere protuberance. *J. Fluid Mech.* **175**, 1–41.

ACARLAR, M. S. & SMITH, C. R. 1987*b* A study of hairpin vortices in a laminar boundary layer. Part 2. Hairpin vortices generated by fluid injection. *J. Fluid Mech.* **175**, 43–83.

BLACKWELDER, R. F. 1978 The bursting process in turbulent boundary layers. *Lehigh Workshop on Coherent Structure in Turbulent Boundary Layers* (ed. C. R. Smith & D. E. Abbott), pp. 211–227.

BOGARD, D. G. & TIEDERMAN, W. G. 1986 Burst detection with single-point velocity measurements. *J. Fluid Mech.* **162**, 389–413.

COLES, D. E. & BARKER, S. J. 1975 Some remarks on a synthetic turbulent boundary layer. In *Turbulent Mixing in Non reactive and Reactive Flows* (ed. S. N. B. Murthy), pp. 285–292. Plenum.

ERSOY, S. & WALKER, J. D. A. 1986 Flow induced at a wall by a vortex pair. *AIAA J.* **24**, 1597–1607.

FALCO, R. E. 1991 A coherent structure model of the turbulent boundary layer and its ability to predict Reynolds number dependence. *Phil. Trans. R. Soc. Lond.* A **336**, 103–129.

HAIDARI, A. H. 1990 Generation and growth of single hairpin vortices. PhD dissertation, Lehigh University.

HAJI-HAIDARI, A. & SMITH, C. R. 1988 Development of the turbulent near-wake of a tapered thick flat plate. *J. Fluid Mech.* **189**, 135–163.

HEAD, M. R. & BANDYOPADHYAY, P. 1981 New aspects of turbulent boundary-layer structure. *J. Fluid Mech.* **107**, 297–337.

HON, T. L. & WALKER, J. D. A. 1987 An analysis of the motion and effects of hairpin vortices. Tech. Rep. FM-11. Department of M.E. and Mech., Lehigh University, Bethlehem, PA.

KIM, H. T., KLINE, S. J. & REYNOLDS, W. C. 1971 The production of turbulence near a smooth wall in a turbulent boundary layer. *J. Fluid Mech.* **50**, 133–160.

KIM, J. 1987 Evolution of a vortical structure associated with the bursting event in a channel flow. *Turbulent Shear Flows, 5* (ed. F. Durst *et al.*), pp. 221–233. Springer.

KLINE, S. J., REYNOLDS, W. C., SCHRAUB, F. A. & RUNSTADLER, P. W. 1967 The structure of turbulent boundary layers. *J. Fluid Mech.* **30**, 741–773.

KRAL, L. D. & FASEL, H. F. 1989 Numerical investigation of the control of the secondary instability process in boundary layers. *AIAA, 2nd Shear Flow Conf., Tucson, Arizona, March 13–16.*

LU, L. J. & SMITH, C. R. 1991 Use of quantitative flow visualization data for examination of spatial-temporal velocity and burst-type characteristics in a turbulent boundary layer. *J. Fluid Mech.* **232**, 303–340.

MATSUI, T. 1980 Visualization of turbulent spots in the boundary layer along a flat plate in a water flow. In *Laminar-Turbulent Transition* (ed. R. Eppler & H. Fasel), pp. 288–296. Springer.

OFFEN, G. R. & KLINE, S. J. 1975 A proposed model of the bursting process in turbulent boundary layers. *J. Fluid Mech.* **70**, 209–228.

PERIDIER, V. J., SMITH, F. T. & WALKER, J. D. A. 1991 Vortex-induced boundary-layer separation. Part 2. Unsteady interacting boundary-layer theory. *J. Fluid Mech.* **232**, 133–165.

PERIDIER, V. J. & WALKER, J. D. A. 1989 Vortex-induced boundary-layer separation. *Tech. Rep.* FM-13. Department of M.E. and Mech., Lehigh University, Bethlehem, PA.

PERRY, A. E. & CHONG, M. S. 1982 On the mechanism of wall turbulence. *J. Fluid Mech.* **119**, 173–217.

PERRY, A. E., HENBEST, S. & CHONG, M. S. 1986 A theoretical and experimental study of wall turbulence. *J. Fluid Mech.* **165**, 163–199.

PERRY, A. E., LIM, T. T. & TEH, E. W. 1981 A visual study of turbulent spots. *J. Fluid Mech.* **104**, 387–405.

ROBINSON, S. K. 1991 Coherent motions in the turbulent boundary layer. *Ann. Rev. Fluid Mech.* **23**, 601–639.

SANKARAN, R., SOKOLOV, M. & ANTONIA, R. A. 1988 Substructures in a turbulent spot. *J. Fluid Mech.* **197**, 389–414.

SCHLICHTING, H. 1979 *Boundary Layer Theory*, pp. 469–470. McGraw-Hill.

SMITH, C. R. 1984 A synthesized model of the near-wall behavior in turbulent boundary layers. *Proc. Eighth Symp. on Turbulence* (ed. G. K. Patterson & J. K. Zakin). University of Missouri-Rolla, Dept of Chem. Engng, Rolla, Missouri.

SMITH, C. R. 1993 Use of kernel experiments for modeling of near-wall turbulence. In *Near-Wall Turbulent Flows* (ed. R. M. C. So, C. G. Speziale & B. E. Launder), pp. 33–42. Elsevier.

SMITH, C. R. & METZLER, S. P. 1983 Characteristics of low-speed streaks in the near-wall region of a turbulent boundary layer. *J. Fluid Mech.* **129**, 27–54.

SMITH, C. R., WALKER, J. D. A., HAIDARI, A. H. & SOBRUN, U. 1991 On the dynamics of near-wall turbulence. *Phil. Trans. R. Soc. Lond.* A **336**, 131–175.

THEODORSEN, T. 1952 Mechanism of turbulence. *Proc. Second Midwestern Conf. of Fluid Mechanics, Ohio State University, Columbus, Ohio*, pp. 1–19.

VAN DOMMELEN, L. L. & COWLEY, S. J. 1990 On the Lagrangian description of unsteady boundary layer separation. Part 1. General theory. *J. Fluid Mech.* **210**, 593–626.

WALLACE, J. M. 1983 On the structure of bounded turbulent shear flow: A personal view. In *Development in Theoretical and Applied Mechanics, XI* (ed. T. J. Chung & G. Karr), p. 509. University of Alabama in Huntsville, Dept of Mech. Engrg., Huntsville, Alabama.

WILLMARTH, W. W. & TU, B. J. 1967 Structure of turbulence of the boundary layer near the wall. *Phys. Fluids* **10**, S137–S137.

WYGNANSKI, I. 1978 On the possible relationship between the transition process and the large coherent structures in turbulent boundary layers. *Lehigh Workshop on Coherent Structure in Turbulent Boundary Layers* (ed. C. R. Smith & D. E. Abbott), pp. 168–193.